Cell-Free Integrated Sensing and Communication for UGV Detection Based on Decomposed Back Projection Algorithm

Zhiqiang Yue
School of Information Science and Engineering
Southeast University
Nanjing, China
1953433751@qq.com

Yongming Huang
School of Information Science and Engineering
Southeast University
Nanjing, China
huangym@seu.edu.cn

Huazhou Hou
Purple Mountain Laboratories
Nanjing, China
houhuazhou@pmlabs.com.cn

Dongxuan He
School of Information and Electronics
Beijing Institute of Technilogy
Beijing, China
dongxuan_he@bit.edu.cn

2024 IEEE International Conference on Unmanned Systems (ICUS) | 979-8-3503-8418-5/24/$31.00 ©2024 IEEE | DOI: 10.1109/ICUS61736.2024.10839755

***Abstract*—This paper considers the localization and velocimetry problem of UGV by integrated sensing and communications in a Sub-6GHz cell-free system. Multiple distributed antennas are used to detect a single target and the echo signals are processed. For the receiver processing algorithm, we develop an improved algorithm suitable for real systems to address the problem that the matched-filter based backprojection algorithm consumes too much time. By decomposing range and velocity, the original algorithm is split into range backprojection and velocity backprojection algorithms respectively, and the effective target is identified by constant alarm false rate (CFAR) algorithm. Simulation results show that the improved algorithm increased the computation speed by at least 100 times. For the real system, better results are achieved by proposed algorithm for localization and velocimetry as well.**

Keywords—integrated sensing and communication, back projection, sub-6GHz, cell-free network, UGV detection

I. INTRODUCTION

With the continuous development of communication technology after 5G, higher frequency bands are used in the communication systems, including millimeter wave (mm-Wave), terahertz (THz), as well as denser arrays of antennas, providing greater communication bandwidth, capacity, and rate. This reflects the fact that communication and radars are developing more and more similarly and the boundaries between them are becoming more and more blurred. This situation have given rise to the Integrated Sensing and Communication (ISAC), which refers to a set of systems with both communication and sensing capabilities, where the two functions are codesigned and integrated into the same set of hardware[1]. The advantages of ISAC are that it can improve the spectrum efficiency and reduce the hardware cost by sharing the frequency band and hardware, and the sensing and communication functions can assist each other to improve the overall performance of the system.

Recently, the signal processing methods of ISAC have been extensively studied in academia, among which the sensing parameters estimation is an important signal processing technique, and it is an essential step in applications such as beam forming[2], target detection [3] and object tracking [4]. Common parameters include: time delay, doppler frequency, angle of arrival (AoA), angle of departure (AoD) and multipath signal strength. Common parameter estimation algorithms include: matched filtering [5], multiple signal classification (MUSIC) [6], estimating signal parameters via rotational invariance techniques (ESPRIT) [2], and compressive sensing [7], and the paper [8] provides a full comparison of the above methods. It should be noted that the algorithms would be implemented and employed in a real system with high limits on the complexity, thus, matched filtering gets our attention because it is simple and easy to implement, as well as it is common in radar signal processing. In addition, most of the current work is based on traditional cellular networks, and little work has been done to study ISAC in cell-free networks relatively. Compared with the cellular networks, the cell-free architecture can increase the spectrum utilization, improve the system coverage and cell boundary performance, and reduce the size and cost of the antenna [9]. Therefore, we will study the ISAC signal processing methods in a cell-free architecture. The paper [10] has proposed an backprojection algorithm and its related improvements in the Sub-6GHz band with OFDM waveforms. However the article does not consider the computation of velocity vectors and the cell-free architecture. On this basis, some improvements have been done, which enables us to carry out the tasks of localization and velocimetry in a cell-free system successfully.

In this paper, we have investigated the localization and velocimetry algorithms for ISAC in a cell-free system employing Sub-6GHz band. The contribution of this paper can be summarized as follows. First of all, the sensing channel model is established for the single target case, and the expression for the received signal is obtained. Next, to address high complexity of the original backprojection algorithm, an improved decomposed algorithm is proposed, including range backprojection and velocity backprojection. And constant false alarm rate algorithm (CFAR) is used to extract the effective target. Finally, the simulation shows that the proposed algorithm can effectively reduce the computation time. The practical UGV detection experiment is performed to verify the algorithms in a semicircular field with one target. The accurate positioning results show the effectiveness of the proposed algorithm in the real system.

979-8-3503-8418-5/24/$31.00 ©2024 IEEE

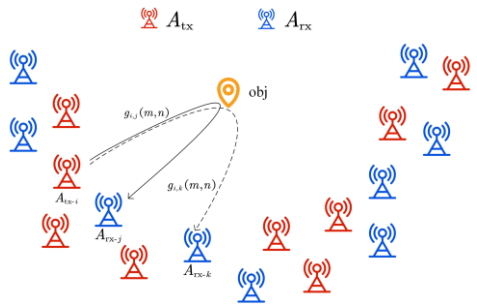

Fig. 1. The bistatic sensing channel with one target.

II. Problem Description And System Model

We consider a cell-free system containing M transmitting antennas and N receiving antennas. All the antennas are connected to the rear building base band unit (BBU) via optical fiber and then the data fusion process is carried out, and this transmission is considered to be error-free. All the transmitter share the same bandwidth and use different orthogonal codes, and the receivers are able to separate the signals from each of the transmitters completely.

In communication systems, OFDM is the most commonly used waveform. Since OFDM signals can achieve high spectral efficiency without implementing complex equalization filters [11], we also choose it as the transmit waveform. The total bandwidth is B, the carrier frequency is f_c. The subcarrier spacing is Δ_f, and the number of subcarriers and symbols are M and N, respectively.

The transmitted signal frame has three components, which are uplink, downlink and special. In order to verify the effectiveness of the sensing algorithm, we fill the special part with the pilot data, and the uplink and downlink segments are not filled with communication data. We use the Zadoff-Chu (ZC) sequence in 3GPP protocol as the pilot data, whose good autocorrelation property has potential sensing capability.

A. OFDM Transmittd Signal

In this subsection, we introduce more OFDM-related details to facilitate the subsequent discussion. For simplicity, only OFDM signals carrying the sensing data is considered here, and we don't insert communication data in the signal for the time being. The bandwidth used by the transmitters is B, and the subcarrier interval is Δ_f, then $B = K\Delta_f$. The number of symbols is N, and the symbol interval is $T_s = T + T_{\text{cp}}$, where $T = 1/\Delta_f$ and T_{cp} is the duration of the cyclic prefix. $m = 1,...,M$ represents the subcarrier index and $n = 1,...,N$ represents the symbol index.

The continuous time domain expression for the transmit signal is:

$$s(t) = \frac{1}{\sqrt{K}} \sum_{n=0}^{N-1} \sum_{m=0}^{M-1} x(m,n) \times e^{j2\pi m\Delta_f (t-nT_s-T_{\text{cp}})} \mathrm{u}_{T_s}(t-nT_s) \tag{1}$$

where u_{T_s} is a rectangular square wave function that is equal to 1 only in [0,1]. $x(m,n)$ is the data in the OFDM resource cells, which is replaced by ZC sequence. The ZC sequence is a kind of discrete complex sequence with constant envelope and good autocorrelation properties, so it can be used to implement sensing. For a ZC sequence of length N_{ZC}, the expression is

$$x_\mu = e^{-j\phi} = e^{-j\frac{\pi\mu i(i+1)}{N_{ZC}}} \tag{2}$$

where: $i = 1,...,N_{ZC}-1$; μ is the physical root sequence index; ϕ is the angle to the coordinate axis.

B. Channel Model

Considering the scenario with one moving target, the propagation channel of the sensing signal is shown in Fig. 1. Since the target is in motion, the sensing channel is modeled as a linear time-varying filter. The set containing transmitters is A_{tx}, and the set containing receivers is A_{rx}. In keep with the paper [12], for $i \in A_{\text{tx}}$, $j \in A_{\text{rx}}$, the m-th subcarrier, and the n-th symbol, the expression for the sensing channel is

$$g_{ij}(m,n) = \alpha_{\text{tx-}i,\text{rx-}j,\text{obj}} e^{-j2\pi m\tau_{\text{tx-}i,\text{rx-}j,\text{obj}}/T} \times e^{-j2\pi n f_{\text{tx-}i,\text{rx-}j,\text{obj}} T_s} \tag{3}$$

where: $\alpha_{\text{tx-}i,\text{rx-}j,\text{obj}}$ is a complex coefficient accounting for the target reflection and path loss; $\tau_{\text{tx-}i,\text{rx-}j,\text{obj}}$ is the bistatic propagation delay via target reflection, equal to $d_{\text{tx-}i,\text{rx-}j,\text{obj}}/c$, in which $d_{\text{tx-}i,\text{rx-}j,\text{obj}}$ is the propagation distance of the signal reflected by the target, and c is the speed of light; $f_{\text{tx-}i,\text{rx-}j,\text{obj}}$ is the bistatic doppler shift, less than the maximum Doppler frequency due to projection: $f_{\text{tx-}i,\text{rx-}j,\text{obj}} \leqslant 2v_{\max} f_c/c$, where $v_{\max}$ is the maximum speed of the target. For convenience, the subscripts $\text{tx-}i,\text{rx-}j,\text{obj}$ will be replaced by i,j,o hereafter.

C. Received Signal

Modeling the channel as a linear time-varying filter $g(t)$, the expression of the received signal can be denoted as $y(t) = s(t)*g(t) + z(t)$, where $z(t)$ is the noise, modeled as a complex circularly symmetric Gaussian process with bandwidth B, and power P_n. Sampling the received signal at $t = nT_s + T_{\text{cp}} + kT/M$, with a total of M points, we can get

$$y(k,n) = \alpha \frac{1}{\sqrt{M}} \sum_{m=0}^{M-1} x(m,n) e^{j2\pi km/M} G(m) + z(k,n) \tag{4}$$

where: $k = 0,...,M-1$ and $n = 0,...,N-1$; $G(m)$ is the Fourier transform of the time-domain filter $g(t)$ sampled at $m\Delta_f$; $z(k,n)$ obeys the distribution $\mathcal{CN}(0,P_n)$. For the above sampling points in the time domain, the DFT is performed, which can be obtained as

$$\begin{aligned} y(m,n) &= \frac{1}{\sqrt{M}} \sum_{m=0}^{M-1} y(k,n) e^{-j2\pi km/M} \\ &= G(m)x(m,n) + z(m,n) \end{aligned} \tag{5}$$

where $z(m,n)$ obeys the distribution $\mathcal{CN}(0,1)$, and is the Fourier transform of $z(t)$. Take (3) into (5):

$$y(m,n) = \alpha x(m,n) e^{-j2\pi m\tau/T} e^{-j2\pi n f_d T_s} + z(m,n) \tag{6}$$

From the above equation, it can be seen that the distance and velocity information of the moving target is included in the phase of the received signal and can be separated independently and easily, which is one of the advantages of

using OFDM to estimate the parameters. In addition, to distinguish the existence of a target, it is necessary to satisfy $|m\tau/T| \leqslant 1$ and $|nf_dT_s| \leqslant 1/2$. Thus, the bistatic distance and velocity resolution can be denoted as $c/(M\Delta f)$ and $c/(NT_sf_c)$, respectively.

III. Signal Processing Algorithms

Next, we discuss the receiver signal processing algorithms for performing target localization in the cell-free network.

A. Matched Filtering

Many research algorithms exist for target localization. Here, the traditional matched filtering algorithm framework is considered for target localization. The advantage of this method is that it is less complexity and more convenient to implement in real systems [8].

1) Range matched filtering: The received signal is propagated with a delay, which is reflected in the frequency domain as a phase change. Therefore, the delay parameter can be extracted by matched filtering.

Performing range matched filtering along the subcarriers:

$$\begin{aligned} R_{ij}^{(r)}(d,n) &= \frac{1}{M}\sum_{m=1}^{M} S_{ij}(m,n)\cdot f_d(d,m) \\ &= \frac{1}{M}\sum_{m=1}^{M} S_{ij}(m,n)\cdot \omega_d(m) e^{j2\pi\frac{\Delta f}{c}dm} \\ &= \frac{\alpha_{i,j,o}}{M}\sum_{m=1}^{M} x_{ij}(m,n)\cdot \omega_d(m)\times e^{-j2\pi f_c\frac{d_{i,j,o}}{c}}\times e^{j2\pi\frac{\Delta f}{c}(d-d_{i,j,o})m} \\ &\quad \times e^{-j2\pi\frac{v_{i,j,o}}{\lambda}nT_p} \end{aligned} \tag{7}$$

where: $f_d(d,m) = \omega_d(m)e^{j2\pi\frac{\Delta f}{c}dm}$; $d_{i,j,o}$ is the bistatic distance; $w_d(m)$ is a window function designed to reduce spectrum leakage. The results will have larger values at the bistatic distance cell where the target exists, through which the value of the distance can be obtained. After the coherent processing by the matched filtering, the energy of the target is accumulated and the signal-to-noise ratio is improved by a factor of K.

2) Velocity matched filtering: The target's velocity causes a frequency shift to the signal, called doppler frequency. Similar to the processing above, velocity matched filtering along the time domain shows as follows.

$$\begin{aligned} R_{ij}^{(d)}(m,v) &= \frac{1}{N}\sum_{n=1}^{N} S_{ij}(m,n)\cdot f_v(n,v) \\ &= \frac{1}{N}\sum_{n=1}^{N} S_{ij}(m,n)\cdot \omega_v(n) e^{j2\pi\frac{v}{\lambda}nT_p} \\ &= \frac{\alpha_{i,j,o}}{N}\sum_{n=1}^{N} x_{ij}(m,n)\cdot \omega_v(n) e^{-j2\pi f_c\frac{d_{i,j,o}}{c}} e^{j2\pi\frac{\Delta f}{c}d_{i,j,o}m} e^{j2\pi\frac{(v-v_{i,j,o})}{\lambda}nT_p} \end{aligned} \tag{8}$$

where: $f_v(n,v) = \omega_v(n)e^{j2\pi\frac{v}{\lambda}nT_p}$; $v_{i,j,o}$ is the bistatic velocity; $w_v(n)$ is a window function.

B. Range and Doppler Map

Combining range and velocity matched filtering, which means doing two consecutive matched filtering along the subcarrier and symbol, respectively, the range-doppler (RD) map can be obtained to get the target's bistatic distance and velocity, which is calculated as follows

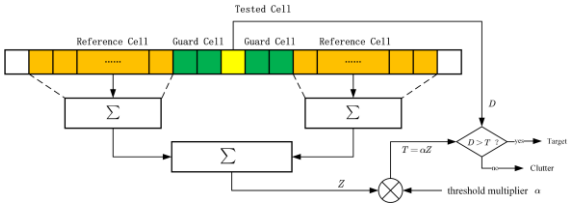

Fig. 2. One-dimentional CFAR structure.

$$\begin{aligned} R_{ij}^{(rd)}(d,v) &= \frac{1}{MN}\sum_{n=1}^{N} R_{ij}^{(d)}(d,l)\cdot\omega(n)\times e^{j2\pi\frac{v}{\lambda}nT_p} \\ &= \frac{\alpha_{i,j,o}}{MN}\sum_{n=1}^{N}\sum_{m=1}^{M} x_{ij}(m,n)\cdot\omega_d(m)\omega_v(n) \\ &\quad \times e^{-j2\pi f_c\frac{d_{i,j,o}}{c}}\times e^{j2\pi\frac{\Delta f}{c}(d-d_{i,j,o})m}\times e^{j2\pi\frac{(v-v_{i,j,o})}{\lambda}nT_p} \\ &= \sum_{n=1}^{N}\sum_{m=1}^{M} A\cdot e^{j2\pi\frac{\Delta f}{c}(d-d_{i,j,o})m}\times e^{j2\pi\frac{(v-v_{i,j,o})}{\lambda}nT_p} \end{aligned} \tag{9}$$

where $A = \alpha_{i,j,o}/MN\cdot\omega_d(m)\omega_v(n)x_{ij}(m,n)e^{-j2\pi f_c\frac{d_{i,j,o}}{c}}$ is a variable-independent term. The range-doppler processing not only converts the symbol-subcarrier domain to the range-velocity domain, which intuitively presents the bistatic distance and velocity as well as number of targets, but also provides KL times coherence gain, which makes the target and the noise easier to distinguish from each other.

C. Constant False Alarm Rate for Target Detection

Classical radar signal processing uses constant false alarm rate (CFAR) for target detection and extraction. By setting an adaptive threshold, real targets can be recognized and valuable parameters can be extracted in a background containing noise and clutter. The false alarm probability P_{fa} is the probability that a peak of noise or clutter is mistaken as a target by the detector. By setting a high P_{fa}, the probability of misdetection is limited to a tolerable level while still allowing the target to be successfully detected.

The CFAR detector consists of three parts: the central unit to be detected, and the guard and reference units on both sides, shown in Fig. 2. The guard unit is located around the unit to be detected and serves to prevent the target signal power from leaking to the reference unit and causing interference. The reference unit is used to estimate the average power of the noise. Considering the framework of Rayleigh-distributed clutter and square-law detector, set up N_r reference cell. Assuming that Z is the average noise power, it is derived from the value of the reference units. The detection threshold is calculated as the product of two terms:

$$T = \alpha Z \tag{10}$$

where α is the detection factor, which reflects the degree of tolerance to clutter. It is associated with the value of false alarm probability and the number of reference cells [13]:

$$\alpha = N_r(P_{\text{fa}}^{-1/N_r} - 1) \tag{11}$$

For each value of the input data, a detection threshold is calculated and compared to judge the existence of the target. Moving the guard unit and the reference unit, the operation is

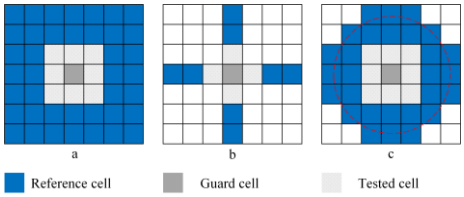

Fig. 3. Two-dimensional reference window shape.

repeated until a judgment is made for each data. Eventually we can gain the set of targets $\Omega = \{t_1, t_2, t_3, \ldots\}$.

For the two-dimensional case, the reference cell can be set as different shapes, such as the three samples in Fig. 3. In terms of complexity and accuracy, the order of the three samples is: circle > rectangle > cross. For the edge part of the input data, the number of reference units is insufficient, which leads to the problem of not being able to calculate. It is possible to consider constructing a complete number of reference units by adding zero units.

D. Decomposed Backprojection Algorithm for Location and Velocimetry

Localization requires the joint signal processing of multiple transceivers. After obtaining the RD map of each transceiver channel, the environment map is generated by fusing all channels through coherent processing. This result allows us to get the coordinates and velocity vectors of the targets. Since the distances and velocities in the RD map are bistatic, they need to be converted into spatial coordinates and velocity vectors first. Denote the bistatic distance by

$$d_{i,j,\mathrm{o}} = d_{\text{tx-}i,\mathrm{obj}} + d_{\text{rx-}j,\mathrm{obj}} \tag{12}$$

where $d_{\text{tx-}i,\mathrm{obj}}$ is the distance from the *i*-th transmitter to the target and $d_{\text{rx-}i,\mathrm{obj}}$ is the distance from the *j*-th receiver to the target. Assuming that the coordinate of the *i*-th transmitter is $(x_{\text{tx-}i}, y_{\text{tx-}i})$, the coordinate of the *j*-th receiver is $(x_{\text{rx-}j}, y_{\text{rx-}j})$, and the coordinate of the target is $(x_{\mathrm{obj}}, y_{\mathrm{obj}})$, then

$$d_{\text{tx-}i,\mathrm{obj}} = \sqrt{(x_{\text{tx-}i} - x_{\mathrm{obj}})^2 + (y_{\text{tx-}i} - y_{\mathrm{obj}})^2} \tag{13}$$

$$d_{\text{rx-}j,\mathrm{obj}} = \sqrt{(x_{\text{rx-}j} - x_{\mathrm{obj}})^2 + (y_{\text{rx-}j} - y_{\mathrm{obj}})^2} \tag{14}$$

Assuming the bistatic velocity is $v_{i,j,\mathrm{o}}$, it can be denoted as

$$v_{i,j,\mathrm{o}} = v_{\text{tx-}i,\mathrm{obj}} + v_{\text{rx-}j,\mathrm{obj}} \tag{15}$$

where $v_{\text{tx-}i,\mathrm{obj}}$ is the projected velocity on the transmitter-target path and $v_{\text{rx-}j,\mathrm{obj}}$ is the target-receiver projected velocity, assuming that the target's velocity is $\boldsymbol{v} = (v_x, v_y)$, then

$$v_{\text{tx-}i,\mathrm{obj}} = \frac{x_{\text{tx-}i} - x_{\mathrm{obj}}}{d_{\text{tx-}i,\mathrm{obj}}} v_x + \frac{y_{\text{tx-}i} - y_{\mathrm{obj}}}{d_{\text{tx-}i,\mathrm{obj}}} v_y \tag{16}$$

$$v_{\text{rx-}j,\mathrm{obj}} = \frac{x_{\text{rx-}j} - x_{\mathrm{obj}}}{d_{\text{rx-}j,\mathrm{obj}}} v_x + \frac{y_{\text{rx-}j} - y_{\mathrm{obj}}}{d_{\text{rx-}j,\mathrm{obj}}} v_y \tag{17}$$

Once we have obtained the above conversion method from bistatic distance and bistatic velocity to coordinate and velocity vectors, the variables in the RD maps can be replaced. Then the spatial data can be derived by means of coherent processing, combining the data from $M \times N$ channels:

$$\begin{aligned} P(x,y,v_x,v_y) &= \left| \sum_{j \in A_{\mathrm{rx}}} \sum_{i \in A_{\mathrm{tx}}} R_{ij}^{(rd)}(d_{ij}(x,y), v_{ij}(x,y,v_x,v_y))\, \overline{p}_{ij}(x,y) \right|^2 \\ &= \left| \sum_{j \in A_{\mathrm{rx}}} \sum_{i \in A_{\mathrm{tx}}} R_{ij}^{(rd)}(x,y,v_x,v_y)\, \overline{p}_{ij}(x,y) \right|^2 \end{aligned} \tag{18}$$

$$\overline{p}_{ij}(x,y) = \exp\left(j \frac{2\pi}{\lambda} d(x,y) \right) \tag{19}$$

$$d(x,y) = d_{i,j,\mathrm{o}}\big|_{\mathrm{obj} = (x,y)} \tag{20}$$

where $\overline{p}_{ij}(x,y)$ is used as the matched filter. Substituting (19) and (20) into (18) and organizing gives the result (21), where $B = \alpha_{i,j,\mathrm{o}}/MN \cdot \omega_d(m)\omega_v(n)x_{ij}(m,n)$ is a variable-independent term. The algorithm is called back-projection, and we have made appropriate simplifications for the method mentioned in [10]. From (21), it can be noted that the maximum value of the result occurs when the given x, y, v_x, v_y is successful matched to the actual bistatic distance and velocity: $d_{i,j,\mathrm{o}}$ and $v_{i,j,\mathrm{o}}$. From the index of the maximum value, we can get the coordinates and velocity vector of the target. By combining all channels, MN times coherence gain can be realized, making the target more conspicuous even in noisy environments. Thus when the number of antennas used for sensing is sufficiently large and the target moves relatively slowly, (21) can effectively utilize the information carried by the signal.

However, (21) needs to search the parameters in a 4-D space, and it is too complex to run in real systems, so the backprojection needs to be simplified. The idea of simplification can be considered from two aspects. Firstly, in order to derive the coordinates of the target, the velocity phase can be ignored temporarily, and only the range matched filtering of multiple channels should be used. For low-speed targets, the distance changed during the processing will be less than a minimum distance cell. Secondly, performing the velocity processing after determining the position of the targets can reduce the number of traversals, i.e., for each target in the set Ω, their velocity vectors are calculated separately. Therefore, the backprojection algorithm can be decomposed into distance backprojection and velocity backprojection. Replacing the RD map in (18) by the range matched filtering result, gives

$$\begin{aligned} P(x,y) &= \frac{1}{N_L} \sum_{n=1}^{N_L} \left| \sum_{j \in A_{\mathrm{rx}}} \sum_{i \in A_{\mathrm{tx}}} R_{ij}^{(r)}(d(x,y), l)\, \overline{p}_{ij}(x,y) \right|^2 \\ &= \frac{1}{N_L} \sum_{n=1}^{N_L} \left| \sum_{j \in A_{\mathrm{rx}}} \sum_{i \in A_{\mathrm{tx}}} R_{ij}^{(r)}(x,y,l)\, \overline{p}_{ij}(x,y) \right|^2 \end{aligned} \tag{22}$$

where N_L is the number of symbols specified for processing, and the cumulative gain can be improved by averaging the results of multiple symbol processing. The above method is called distance backprojection, which extracts coordinates

$$P(x,y,v_x,v_y) = \left| \sum_{j \in A_{\mathrm{rx}}} \sum_{i \in A_{\mathrm{tx}}} \sum_{n=1}^{N} \sum_{m=1}^{M} B e^{j2\pi \frac{\Delta f}{c}(d(x,y) - d_{i,j,\mathrm{o}})m} e^{j2\pi \frac{(v(x,y) - v_{i,j,\mathrm{o}})}{\lambda} n T_p} e^{j\frac{2\pi}{\lambda}(d(x,y) - d_{i,j,\mathrm{o}})} \right|^2 \tag{21}$$

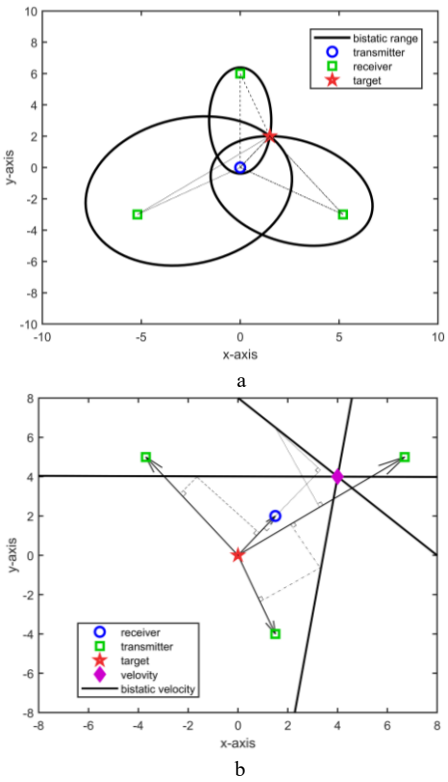

Fig. 5. Physical significance of distance and velocity backprojection.

only from distance information. The algorithm also has a clear physical meaning, as shown in Fig. 4a. For bistatic sensing, the result of the range matched filtering is projected to the planar coordinates as an ellipse, and in combination with all channels, multiple ellipses will intersect to a point where lies the target. After CFAR processing, all coordinates can be extracted $\Omega = \{(x_1,y_1),(x_2,y_2),...\}$. For each target, use the velocity matched filtering result $R_{ij}^{(d)}$ for incoherent combining, and perform the velocity backprojection as follows.

$$V(v_x,v_y)|_{(x,y)\in\Omega} = \frac{1}{N_M}\sum_{m=1}^{N_M}\sum_{j\in A_{tx}}\sum_{i\in A_{tx}}|R_{ij}^{(d)}(k,v_{ij}(x,y))|^2 = \frac{1}{N_M}\sum_{m=1}^{N_K}\sum_{j\in A_{tx}}\sum_{i\in A_{tx}}|R_{ij}^{(d)}(k,v_x,v_y)|^2 \quad (23)$$

$$\boldsymbol{v} = arg\max_{v_x,v_y} V(v_x,v_y)|_{(x,y)\in\Omega} \quad (24)$$

where N_K is the number of subcarriers processed and the cumulative gain can be obtained by averaging. Since the velocity of the object is unique, the index of the maximum is the velocity vector. The physical significance of the velocity backprojection is shown in Fig. 4b. In order to make the sum of the velocity projected to the transmitter and receiver a fixed value, the potential target velocities comprise a set of straight lines. For bistatic velocity, and the velocity of the target is where the three straight lines intersect at one point.

IV. Performance Analysis of Improved Algorithm

In this section, the performance of the backprojection and its improved version is analyzed below. In order to check the sensing capability of the system, we have taken the number of processing symbols and subcarriers, and processing time as

Fig. 4. Outdoor experimental site layout (including the coordinates of the transceiver and the track of the object).

TABLE I. Main Simulation Parameters

Name	Value	Description
f_c	4.9 GHz	carrier frequency
M	3276	number of subcarriers
N	800	number of processed symbols
T_c	1.25 ms	time slot duration
Δ_f	30 kHz	subcarrier spacing

the key performance metrics. First of all, to show the performance enhancement brought by the decomposed distance and velocity backprojection, the processing time is compared with that of the original backprojection under different simulation settings. Then, the experiments are carried out in an outdoor testbed, where the environment map is constructed and the target is localized. Table I gives the necessary parameters used in the experiments.

Firstly, the processing time of different algorithms is recorded. Two transmitters and two receivers are set up on a 20×20 square plane, which are sequentially distributed at the midpoints of the field edges. For simplicity, there is a moving target inside the area with coordinates (6,12) m and velocity magnitude of 2.83 m/s. The coordinates and velocity of the target are computed using the original backprojection algorithm, which consumes 265.818 s. The processing time of the improved algorithm is recorded for the case of dealing with different number of subcarrier and symbol, including $L=1$, $K=1$ and $L=40$, $K=40$ and $L=80$, $K=80$ and $L=120$, $K=120$ and $L=160$, $K=160$ and $L=200$, $K=200$, with multiple experiments averaged for each group. The processing time of distance backprojection-CFAR detection-velocity backprojection is finally recorded and the results are displayed in Table II. It can be found that the classic backprojection algorithm takes a lot of time and it is not suitable for application in real systems. By using the improved decomposed algorithms, the computation speed can be increased by at least 100 times. As L and K increase, the processing time also increases, but the detection signal-to-noise ratio can be improved furtherly.

Experiments are also conducted in an outdoor site shown in Fig. 5. Inside a semi-circular arc with a radius of 30 m, one transmitter and seven receivers are set up, where the transmitter is located at the center of the circle and seven

TABLE II. CALCULATION TIME WITH DIFFERENT SETTINGS

	Distance backprojection–CFAR–Velocity backprojection		
time	$L=1, K=1$	$L=40, K=40$	$L=80, K=80$
	0.189 s	0.511 s	1.308 s
	$L=120, K=120$	$L=160, K=160$	$L=200, K=200$
	1.608 s	2.202 s	2.814 s

receivers are distributed on the semi-circular arc. All transceivers are connected to the BBU and switch via optical fiber and network cable for unified data processing. A moving target traverses the entire field with a speed of 1.5 m/s on a y = 5 m path, and the path is shown as the blue line in Fig. 5. The transmitter continuously emits signals to track the target, and the seven receivers record data from all channels. Two moments of entry and exit are selected for data processing due to the severe direct path signals inside the semicircular region, which caused sticky interference with data processing. The results using the improved decomposed algorithms are shown in Fig. 6. The CFAR detection is able to recognize moving target and label it with triangles. Due to resolution limitations, multiple triangles are used to represent a single target. Using the velocity backprojection, the results are shown in Fig. 6c and Fig. 6d. The results are (3.3,0.2) m/s and (0.3,0.7) m/s respectively. It is worth noting that there is a certain discrepancy between the results and the real velocities, caused by carrier frequency offset possibly, which leads to a lack of accuracy in the velocimetry. In the further study, we will consider the influence of frequency offset on positioning and find ways to eliminate it.

V. CONCLUSIONS

This paper considers the problem of localization and velocimetry for UGC with ISAC in sub-6GHz cell-free networks. First, a complete signal model is given considering the effects of sensing parameters. Then the receiver signal processing algorithms for localization and velocimetry are derived. Aiming at the problem that the classic back-projection algorithm is time-consuming, the decomposed distance and velocity backprojection algorithms are proposed. The coordinates of the effective target are first extracted by distance backprojection and CFAR, and then the velocity vector is obtained using velocity backprojection. Simulation results show that the decomposed algorithm can increase the processing speed by at least 100 times. The algorithm is applied to a real platform, and the target is successfully localized. A solution to the problem of frequency offset causing inaccuracy to the results will also be conducted in the subsequent research.

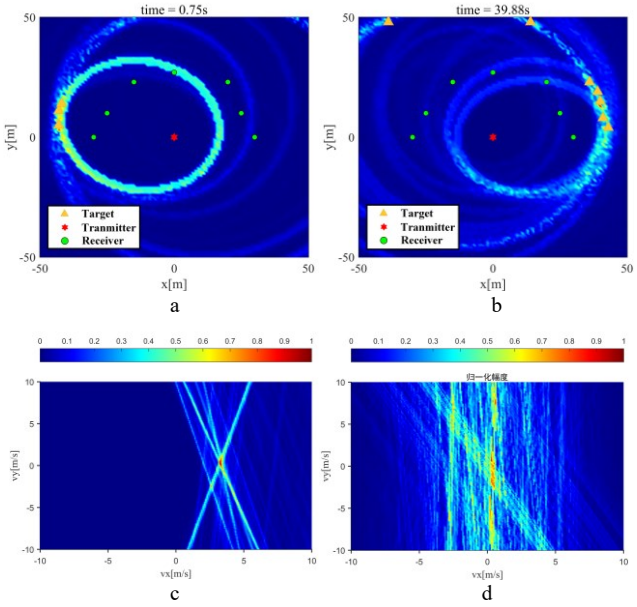

Fig. 6. Target positioning and velocity results for entering and leaving the area.

REFERENCES

[1] J. A. Zhang, R. W. Heath, Z. Feng, and A. Petropulu, "An overview of signal processing techniques for joint communication and radar sensing," *IEEE J. Sel. Top. Signal Process.*, vol. 15, no. 6, pp. 1295-1315, Nov. 2021.

[2] S.-F. Chuang, W.-R. Wu, and Y.-T. Liu, "High-Resolution AoA Estimation for Hybrid Antenna Arrays," *IEEE Trans. Antennas Propag.*, vol. 63, no. 7, pp. 2955–2968, Jul. 2015.

[3] A. M. Haimovich, R. S. Blum, and L. J. Cimini, "MIMO radar with widely separated antennas," *IEEE Signal Process. Mag.*, vol. 25, no. 1, pp. 116–129, Dec. 2007.

[4] S. Sen and A. Nehorai, "Sparsity-Based Multi-Target Tracking Using OFDM Radar," *IEEE Trans. Signal Process.*, vol. 59, no. 4, pp. 1902–1906, Apr. 2011.

[5] P. Kumari, J. Choi, N. Gonzalez-Prelcic, and R. W. H. Jr, "IEEE 802.11ad-Based Radar: An Approach to Joint Vehicular Communication-Radar System," *IEEE Trans. Veh. Technol.*, vol. 67, no. 4, pp. 3012-3027, Apr. 2018.

[6] Y. Liu, G. Liao, Y. Chen, J. Xu, and Y. Yin, "Super-Resolution Range and Velocity Estimations With OFDM Integrated Radar and Communications Waveform," *IEEE Trans. Veh. Technol.*, vol. 69, no. 10, pp. 11659-11672, Oct. 2020.

[7] Md. L. Rahman, J. A. Zhang, X. Huang, Y. J. Guo, and R. W. Heath, "Framework for a Perceptive Mobile Network Using Joint Communication and Radar Sensing," *IEEE Trans. Aerosp. Electron. Syst.*, vol. 56, no. 3, pp. 1926–1941, Jun. 2020.

[8] M. L. Rahman, J. A. Zhang, X. Huang, Y. J. Guo, and Z. Lu, "Joint communication and radar sensing in 5G mobile network by compressive sensing," *IET Commun.*, vol. 14, no. 22, pp. 3977–3988, Dec. 2020.

[9] D. Wang, J. Wang, X. You, Y. Wang, M. Chen, and X. Hou, "Spectral Efficiency of Distributed MIMO Systems," *IEEE J. Sel. Areas Commun.*, vol. 31, no. 10, pp. 2112–2127, Oct. 2013.

[10] A. Sakhnini, S. De Bast, M. Guenach, A. Bourdoux, H. Sahli, and S. Pollin, "Near-Field Coherent Radar Sensing Using a Massive MIMO Communication Testbed," *IEEE Trans. Wirel. Commun.*, vol. 21, no. 8, pp. 6256–6270, Aug. 2022.

[11] P. Kumari, S. A. Vorobyov, and R. W. Heath, "Adaptive virtual waveform design for millimeter-wave joint communication–radar," *IEEE Trans. Signal Process.*, vol. 68, pp. 715–730, Apr. 2020.

[12] Y. Y. Chu, M. Shakiba-Herfeh, M. Kamoun, E. Grossi, and S. Buzzi, "Integrated sensing and communication in user-centric cell-free massive MIMO systems with OFDM modulation," in *2023 IEEE 34th Annual International Symposium on Personal, Indoor and Mobile Radio Communications (PIMRC)*, IEEE, 2023, pp. 1–7.

[13] M. A. Richards, J. Scheer, W. A. Holm, and W. L. Melvin, *Principles of Modern Radar: Basic Principles*. London, U.K.: Institution of Engineering and Technology, Jan. 2010.